Journal of Cystic Fibrosis 15 (2016) 34 – 42

Journal of Cystic Fibrosis

www.elsevier.com/locate/jcf

Original Article

The impact of Cystic Fibrosis Transmembrane Regulator Disruption on cardiac function and stress response

Kai Jiang [a,f], Sen Jiao [a,f], Megan Vitko [b], Rebecca Darrah [b], Chris A. Flask [a,c,d,f], Craig A. Hodges [b,d], Xin Yu [a,c,e,f,*]

[a] Department of Biomedical Engineering, Case Western Reserve University, Cleveland, OH, USA
[b] Department of Genetics and Genome Sciences, Case Western Reserve University, Cleveland, OH, USA
[c] Department of Radiology, Case Western Reserve University, Cleveland, OH, USA
[d] Department of Pediatrics, Case Western Reserve University, Cleveland, OH, USA
[e] Department of Physiology and Biophysics, Case Western Reserve University, Cleveland, OH, USA
[f] Case Center for Imaging Research, Case Western Reserve University, Cleveland, OH, USA

Received 7 February 2015; revised 10 June 2015; accepted 10 June 2015
Available online 25 June 2015

Abstract

Background: Altered cardiac function has been observed in cystic fibrosis transmembrane regulator (CFTR) knockout mice. However, whether this alteration is a direct effect of CFTR disruption in the heart, or is secondary due to systemic loss of CFTR, remains to be elucidated.
Methods: Cardiac function of mice with muscle-specific or global knockout of CFTR was evaluated at baseline and under β-stimulation by MRI *in vivo*. Myocyte contractility and Ca^{2+} transients were measured in vitro.
Results: Both CFTR knockout models showed increased twist and torsion at baseline. Response to β-stimulation was unaltered in muscle-specific CFTR knockout mice and was slightly decreased in global CFTR knockout mice. Aortic diameter was also decreased in both mouse models. No difference was observed in myocyte contractility and Ca^{2+} transients.
Conclusions: CFTR disruption leads to increased myocardial contractility at baseline, which may trigger untoward myocardial remodeling in CF patients that is independent of lung diseases.

Keywords: cystic fibrosis; CFTR; left ventricular function; β-adrenergic stimulation; cardiac myocyte

1. Introduction

Cystic fibrosis (CF) is the most common life-shortening autosomal recessive disorder in Caucasians [1]. It results from mutations in the gene encoding the cystic fibrosis transmembrane conductance regulator (CFTR). CFTR functions primarily as a cAMP-activated and ATP-gated chloride channel. Mutations in CFTR lead to premature degradation or reduced capacity of CFTR, causing abnormal ion homeostasis and subsequently hyperviscous secretions in the respiratory and gastrointestinal tracts [2]. Clinical manifestations of CF include chronic airway obstruction, exocrine pancreatic insufficiency, intestinal malabsorption, and infertility [1]. The leading cause of morbidity and mortality in CF is the progressive pulmonary disease. Thanks to the interventions in treating airway obstruction, infection, inflammation, and mucociliary clearance defects, the life expectancy for CF patients has been significantly improved in the last few decades [3]. As a result, CF is now considered a chronic disease of adolescents and adults.

Besides being expressed in epithelia, CFTR was also found in ventricular myocytes of several mammalian species, including mice, rats, swine, simians, and humans [4–7]. It was suggested that CFTR may play a role in maintaining the resting membrane

* Corresponding author at: Wickenden 430, 10900 Euclid Avenue, Cleveland, OH, 44106. Tel.: +1 216 368 3918; fax: +1 216 368 4969.
E-mail address: xin.yu@case.edu (X. Yu).

http://dx.doi.org/10.1016/j.jcf.2015.06.003
1569-1993/

potential and regulating the action potential duration, as well as in minimizing the depolarizing effect of Ca^{2+} entry upon β-adrenergic stimulation [8]. An *ex vivo* study on isolated perfused hearts of CFTR-knockout mice also suggests the involvement of CFTR in mediating ischemic preconditioning [9]. In addition, CFTR was found down-regulated in patients with heart failure [10]. Despite these findings, a complete understanding of the physiological role of CFTR in the heart remains elusive. Clinical studies on CF patients have reported right-ventricular abnormalities caused by pulmonary hypertension [11–13]. Decreased septal and lateral strain rates were also observed in CF patients and were found to correlate with the severity of pulmonary impairment [14]. Due to the presence of lung disease, it is not clear whether these observed changes in ventricular function are a mere response to pulmonary dysfunction or a direct impact from CFTR disruption in the heart.

Unlike CF patients, CFTR knockout mice do not spontaneously develop CF-like pulmonary disease [15] and have been used to investigate the direct impact of CFTR disruption on cardiac function [16,17]. In a recent study on isolated neonatal myocytes, Sellers *et al*. observed decreased contraction rate and increased Ca^{2+} uptake via the L-type Ca^{2+} channels in the presence of a CFTR inhibitor [16]. Further investigation also showed increased ventricular pressure and decreased contractile reserve in response to β-adrenergic stimulation in adult CFTR knockout mice [17]. In addition, changes in myocardial wall thickness and LV chamber size were also observed. However, how these changes impact regional myocardial wall deformation and global functional indexes remains to be elucidated. In addition, it is also not clear whether these changes can be directly attributed to altered myocyte contractility due to CFTR disruption in myocytes or whether these changes in cardiac function are due to a systemic loss of CFTR and are secondary to CF complications.

In the current study, we investigated the impact of CFTR disruption on cardiac function in two mouse models with either muscle-specific or global knockout of CFTR. Global ventricular function and regional myocardial wall motion were evaluated *in vivo* by magnetic resonance imaging (MRI) [18]. Myocyte contractility and Ca^{2+} transients were also measured *in vitro* in isolated ventricular myocytes. All studies were conducted at baseline and under β-adrenergic stimulation. Our results showed that CFTR disruption caused altered ventricular function at baseline independent of systemic loss of CFTR.

2. Materials and Methods

2.1. Animals

Two CF mouse models were utilized in this study. The $CFTR^{tm1Unc}$-knockout mice (referred as CFTR-KO^{GL}) carry a systemic or globally nonfunctional allele of CFTR as previously described [19]. Mice with deletion of CFTR in cardiomyocytes were derived from breeding mice carrying the conditional CFTR-knockout allele ($CFTR^{fl10}$ or $CFTR^{tm1Cwr}$) [15] with mice carrying a transgene expressing Cre recombinase from a smooth muscle protein 22 alpha (SM22α) promoter (JAX strain 004748; [20]). Cre recombinases in these animals are expressed in vascular smooth muscle as well as cardiac myocytes, leading to a muscle-specific CFTR-knockout mouse model (referred as CFTR-KO^{MS}). Inactivation of CFTR in cardiomyocytes was verified on the DNA and RNA levels (Supplemental Fig. 1). CFTR expression was not affected in skeletal muscle of this CF model.

Animals were housed in standard polysulfone microisolator cages in ventilated units with corncob bedding. Mice were given *ad libitum* access to chow (Harlan Teklad 3000; Harlan Teklad Global Diets, Madison, WI) and sterile water. To prevent intestinal obstruction, water with colyte was provided to CFTR-KO^{GL} mice. Regular water was provided to CFTR-KO^{MS} mice. All animals were maintained on a 12-h light, 12-h dark schedule at a mean ambient temperature of 22 °C. 2 ~ 3 month male mice and their age-matched control littermates ($CNTR^{GL}$ and $CNTR^{MS}$, respectively) were used. All animal protocols were approved by the Institutional Animal Care and Use Committee of Case Western Reserve University.

2.2. In Vivo Cardiac Function by MRI

MRI experiments were performed on both CF models and their age-matched control littermates (n = 10 for each group). All mice were first imaged at baseline and then under β-adrenergic stimulation induced by intravenous administration of dobutamine (40 μg/kg/min, Sigma-Aldrich, Bellefonte, PA). Specifically, mice were anesthetized with 2% isoflurane and maintained with 1-2% isoflurane in prone position. A 26G × 19 mm plastic IV catheter (Hospira, Inc., Lake Forest, IL) was inserted into the tail vein and connected to an infusion pump (Braintree Scientific, Inc., Braintree, MA) for dobutamine infusion. ECG, respiration, and body temperature were monitored and recorded by a physiological monitoring system (SA Instruments, Stony Brook, NY). Hot air was blown to the mice to maintain the body temperature at around 36 °C.

All MRI studies were performed on a horizontal 9.4 T scanner (Bruker Biospin, Billerica, MA) with a 35 mm volume coil. Long-axis Cine images of both four-chamber and two-chamber views were acquired. Three short-axis slices located at the basal, mid-ventricular, and apical levels were imaged with an inter-slice distance of 1.5 mm. Two-dimensional myocardial wall motion was quantified in all three slices using the multiphase displacement-encoding with stimulated-echo (DENSE) MRI as described previously [21]. Briefly, for each slice, a total of four sets of DENSE images encoding myocardial wall motion in two orthogonal directions were acquired. For each direction, two sets of images were acquired with the same magnitude of displacement encoding/unencoding gradients but opposite polarities to correct for background phase errors. A displacement encoding frequency at 1.11 cycles/mm was used. 128 points were acquired in the read-out direction and 48 lines at the center of k-space were acquired in the phase-encoding direction to cover the stimulated echo. An average number of 10 was used to achieve desirable signal-to-noise. Other imaging parameters were: flip angle, 30°; slice thickness, 1.0 mm; FOV, 3x3 cm^2; echo time, 2.2 ms. Repetition time was adjusted such that 13 frames were acquired

spanning the entire cardiac cycle. Cine images of all three slices were also acquired to quantify global cardiac function.

2.3. Image Analysis

Images were reconstructed and analyzed off-line using an in-house developed software package in Matlab (The Mathworks, Natick, MA). The inner diameter of the ascending aorta was measured on the four-chamber and two-chamber Cine images. LV endocardial and epicardial contours were traced manually on short-axis Cine images by one expert blinded about the mouse genotype. LV wall thickness, volume, and LV diameter were calculated (Fig. 1a). To ensure accuracy and robustness, the measurement was performed twice and the average value was used. Ejection fraction (EF) was subsequently calculated from the end-diastolic and end-systolic volumes as previously described [22].

Quantification of the displacement, strain, and torsion from DENSE images has been described in detail previously [21]. Briefly, a band-pass filter with a cutoff frequency of 0.90 cycles/mm in the phase-encoding direction was used to select the stimulated echo. The filtered data were then zero filled to a 128x128 matrix in k-space, followed by inverse Fourier transform to generate the complex images in the spatial domain. Displacement-encoded phase images were calculated by subtracting the two phase images acquired using the same encoding gradient but with opposite polarities. Subsequently, phase unwrapping was performed and the 1D displacement for each imaging pixel was calculated. The 2D displacement map was then calculated from vector addition of two individual 1D maps. Subsequently, the Lagrangian strain tensor (E) was computed using the finite-element analysis method [23]. In addition to the strains, LV twist and torsion were also quantified based on the 2D displacement map.

2.4. Myocyte Contractility and Ca^{2+} Transients

Mice were intraperitoneally injected with heparin (1000 units/kg) and sacrificed with cervical dislocation. Hearts were quickly excised, cannulated, and perfused with Ca^{2+}-free Tyrode solution to wash out the blood. The Tyrode solution contained (in mM): NaCl, 136; KCl, 5.4; $MgCl_2$, 1.0; HEPES, 10; NaH_2PO_4, 1.2; glucose, 5.6 mM; L-glutamine, 2; taurine, 5. The pH of the solution was adjusted to 7.4 with NaOH. Afterwards, hearts were perfused with Tyrode solution containing 0.8 mg/mL collagenase type II (Worthington Biochemical Co., Lakewood, NJ) for 8 ~ 10 min. The ventricles were removed from the perfusion column, minced, gently agitated and rinsed. Isolated myocytes were collected and stored in Media 199 (GIBCO, Grand Island, NY) containing 1.8 mM Ca^{2+}. All experiments were conducted with temperature maintained at 36 °C.

Myocyte contractility and Ca^{2+} transients were measured at baseline (n = 13 for $CNTR^{MS}$, 9 for $CFTR\text{-}KO^{MS}$, 10 for $CNTR^{GL}$, and 8 for $CFTR\text{-}KO^{GL}$) and under stress (n = 10 for $CFTR^{MS}$, 8 for $CFTR\text{-}KO^{MS}$, 10 for $CNTR^{GL}$, and 8 for $CFTR\text{-}KO^{GL}$) induced by 100 nM isoproterenol. Isolated myocytes were placed in a glass-bottomed Petri dish on the stage of an Olympus IX71 inverted fluorescence microscope (Olympus America, Center Valley, PA). Myocytes were stimulated at 1-Hz using a Grass stimulator (Grass Technologies, Warwick, RI). A video-edge detector was used to capture the changes in cell length during stimulation. Myocyte contractility

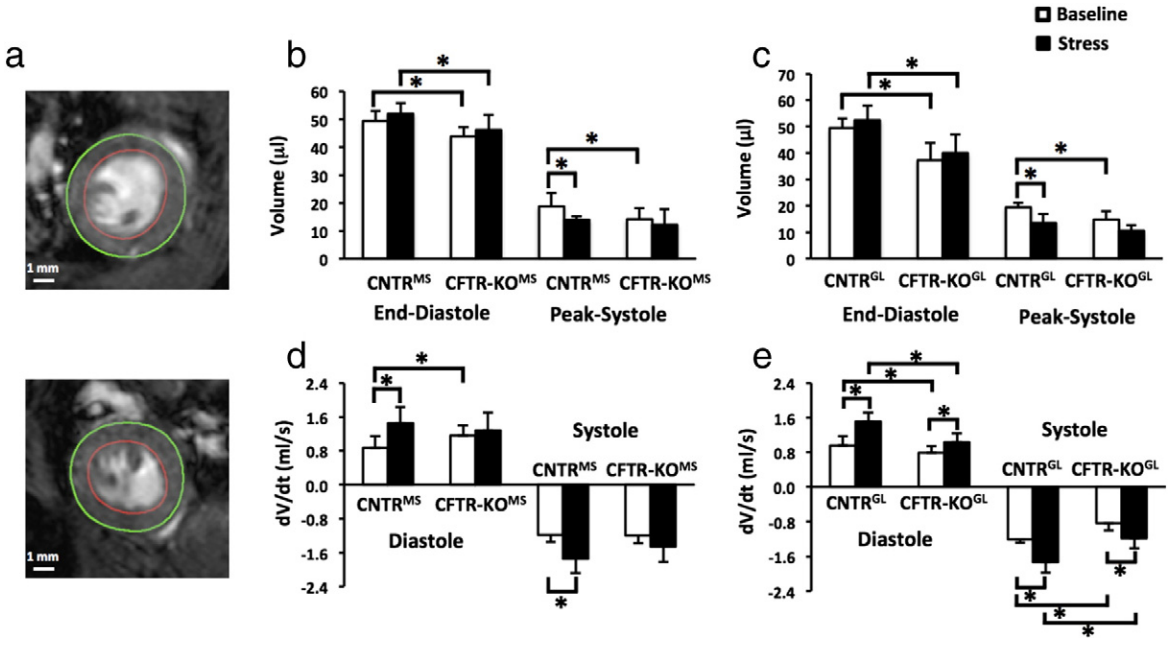

Fig. 1. **Left-ventricular volume by Cine MRI**. **a**. Representative Cine images of one mid-ventricular slice in $CNTR^{MS}$ (**upper**) and $CFTR\text{-}KO^{MS}$ (**lower**) mice at end-diastole. **b&c**. LV volume at end-diastole and peak-systole in $CFTR\text{-}KO^{MS}$ (**b**) and $CFTR\text{-}KO^{GL}$ (**c**) mice and their respective controls. **d&e.** Peak rate of LV volume change at diastole and systole in $CFTR\text{-}KO^{MS}$ (**d**) and $CFTR\text{-}KO^{GL}$ (**e**) mice and their respective controls. *P < 0.05.

was quantified by calculating the maximum fractional shortening in cell length during stimulation. Time to peak shortening was also quantified.

To measure Ca^{2+} transients, myocytes were incubated with 2.5 μM fura-2-acetoxymethyl ester for 20 min, and the extra dye in the media was washed out. The dye was excited at 340 and 380 nm respectively using a xenon arc lamp through a computer-controlled high-speed random access monochromator (Photon Technology International, Birmingham, NJ). The fluorescent signals were detected at 510 nm by an analog/photon counting photomultiplier detector. Ca^{2+} concentration was calculated as the ratio of the detected fluorescence in response to 340 and 380-nm excitation wavelengths (F340/F380), respectively, using in-house-developed MATLAB software. Intracellular Ca^{2+} decay constant (tau) during relaxation was also quantified by a mono-exponential curve fitting.

2.5. Statistical Analysis

All results were expressed as mean ± standard deviation (SD). Unpaired Student's t-test was used for all statistical comparisons between the CF mice and the corresponding controls. Paired Student's t-test was performed in comparison between baseline and β-stimulation. A P value less than 0.05 was considered statistically significant.

3. Results

3.1. Animal Characteristics, LV Structure, and Global Contractile Indexes

The animal characteristics, LV structure, and global contractile indexes are shown in Table 1 and Fig. 1. The CFTR-KO^{MS} mice showed similar body weight but a trend of decrease in heart weight and heart weight to body weight ratio compared to their age-matched controls. The aortic diameter in the CFTR-KO^{MS} mice was also significantly decreased. LV length and wall thickness at end-diastole were similar between the CFTR-KO^{MS} mice and the controls. LV diameter at the mid-ventricular level decreased slightly in the CFTR-KO^{MS} mice ($p < 0.05$). End-diastolic LV volume was significantly decreased in the CFTR-KO^{MS} mice ($p < 0.05$).

The CFTR-KO^{GL} mice showed retarded growth and a significant decrease in both body weight (by 21%, $p < 0.05$) and heart weight (by 12%, $p < 0.05$). Due to a greater decrease in body weight, the heart weight to body weight ratio was slightly increased in CFTR-KO^{GL} mice ($p < 0.05$). Compared to the controls, the CFTR-KO^{GL} mice showed decreased aortic diameter, LV diameter and length ($p < 0.05$). As a result, the LV volume of the CFTR-KO^{GL} mice was significantly decreased ($p < 0.05$). In addition, end-diastolic wall thickness was also decreased in CFTR-KO^{GL} mice ($p < 0.05$).

Table 1
Animal Characteristics and Morphological Indexes (n = 10 for each group).

	CNTR^{MS}	CFTR-KO^{MS}	CNTR^{GL}	CFTR-KO^{GL}
Body weight (g)	26.2 ± 1.8	25.7 ± 1.2	26.3 ± 1.4	20.9 ± 1.5 *
Heart weight (mg)	178.4 ± 11.2	163.7 ± 8.0	165.4 ± 4.1	145.5 ± 6.0 *
Heart weight to body weight ratio (mg/g)	6.8 ± 0.6	6.4 ± 0.5	6.4 ± 0.4	7.1 ± 0.3 *
Aortic diameter (mm)	1.27 ± 0.06	1.12 ± 0.06 #	1.28 ± 0.05	0.97 ± 0.08 *
LV diameter (mm)	4.2 ± 0.2	4.0 ± 0.2 #	4.0 ± 0.3	3.7 ± 0.3 *
LV length (mm)	7.0 ± 0.2	6.9 ± 0.2	6.9 ± 0.4	6.4 ± 0.4 *
End-diastolic wall thickness (mm)	0.75 ± 0.06	0.74 ± 0.05	0.74 ± 0.06	0.64 ± 0.07 *
Peak-systolic wall thickness (mm)				
Baseline	1.29 ± 0.13	1.33 ± 0.14	1.24 ± 0.13	1.07 ± 0.14
Stress	1.46 ± 0.15 †	1.43 ± 0.21	1.43 ± 0.15 †	1.24 ± 0.15 *,†
Increase (%)	17.2 ± 6.0	9.9 ± 8.0	15.9 ± 8.7	15.4 ± 7.9
Heart rate (beats/min)				
Baseline	619 ± 44	625 ± 25	633 ± 26	603 ± 34 *
Stress	658 ± 31 †	643 ± 29	666 ± 38 †	657 ± 22 †
Increase (%)	6.6 ± 5.6	4.7 ± 4.2	6.1 ± 3.0	8.5 ± 6.7
Stroke volume (μl)				
Baseline	30.4 ± 3.1	29.7 ± 2.7	30.4 ± 2.9	23.2 ± 4.9 *
Stress	37.0 ± 4.3 †	33.3 ± 2.6 #,†	37.9 ± 4.0 †	27.1 ± 4.2 *
Increase (%)	19.0 ± 3.5	12.4 ± 6.3 #	21.4 ± 5.9	17.8 ± 4.5
Ejection Fraction (%)				
Baseline	64.4 ± 3.9	70.1 ± 6.7 #	65.0 ± 3.9	63.2 ± 4.9
Stress	76.7 ± 4.5 †	74.3 ± 8.8	77.2 ± 3.8 †	73.8 ± 3.1 *,†
Increase (%)	16.4 ± 3.1	5.6 ± 5.2 #	19.5 ± 4.6	16.4 ± 5.9
Cardiac output (ml/min)				
Baseline	18.5 ± 2.4	18.5 ± 2.3	18.6 ± 2.5	14.2 ± 2.9 *
Stress	24.2 ± 2.7 †	21.3 ± 2.0 #,†	24.7 ± 3.3 †	17.8 ± 2.5 *,†
Increase (%)	33.4 ± 6.9	16.8 ± 2.9 #	32.9 ± 8.3	25.0 ± 5.1

# $P < 0.05$ compared to CNTR^{MS}.
* $P < 0.05$ compared to CNTR^{GL}.
† $P < 0.05$ compared to the baseline.

At baseline, the CFTR-KO^{MS} mice showed a slight increase in ejection fraction as compare to the controls ($p < 0.05$). The CFTR-KO^{MS} mice also showed a higher rate of ventricular filling (dV/dt) at baseline ($p < 0.05$). Despite a slightly smaller LV cavity, the CFTR-KO^{MS} mice showed similar stroke volume as compared to the controls. Heart rate for the CFTR-KO^{MS} mice was also similar to the controls. Consequently, cardiac output in the CFTR-KO^{MS} mice was unchanged. The CFTR-KO^{GL} mice showed a 23.7% decrease in stroke volume and a 5% decrease in heart rate ($p < 0.05$). As a result, cardiac output was also significantly decreased ($p < 0.05$). In contrast to the CFTR-KO^{MS} mice, the CFTR-KO^{GL} mice showed a decreased rate of ventricular filling at diastole, as well as a decreased rate of ejection at systole ($p < 0.05$).

Cardiac stress induced a significant increase in ventricular contractility and heart rate in both CFTR-KO mice and their controls. CFTR-KO^{MS} mice showed similar ejection fraction as the controls, but a slight decrease in stroke volume and cardiac output ($p < 0.05$). Compared to the controls, CFTR-KO^{MS} mice showed less percentage increase in stroke volume, ejection fraction, and cardiac output under β-stimulation. CFTR-KO^{GL} mice showed decreased ejection fraction and systolic wall thickening ($p < 0.05$), suggesting attenuated response to β-adrenergic stimulation as compared to the controls. However, the percentage differences were the same as the controls, primarily due to a decrease in baseline function.

3.2. Myocardial Wall Strain

Representative maps of radial strain at peak-systole are shown in Fig. 2a, with the average peak systolic strain at basal and apical levels shown in Fig. 2b and c, respectively. At baseline, the CFTR-KO^{MS} mice showed increased radial strain at both basal and apical levels ($p < 0.05$), while the CFTR-KO^{GL} mice showed similar radial strain as compared to their control littermates.

Consistent with the observation that ejection fraction was similar between the CFTR-KO^{MS} mice and the controls under β-stimulation, radial strain in CFTR-KO^{MS} mice during β-stimulation was also similar to that of the controls at both the basal and apical levels. On the contrary, the CFTR-KO^{GL} mice showed a significantly decreased apical strain under β-stimulation, which was also consistent with the observed decrease in ejection fraction by cine MRI.

Circumferential strain was similar between the controls and the CFTR-KO mice for both CF models, both at baseline and under cardiac stress (data not shown).

3.3. Ventricular Twist and Torsion

Shown in Fig. 2d are representative displacement maps at the basal and apical levels. LV showed clockwise twist at the basal level but counter-clockwise twist at apex, giving rise to

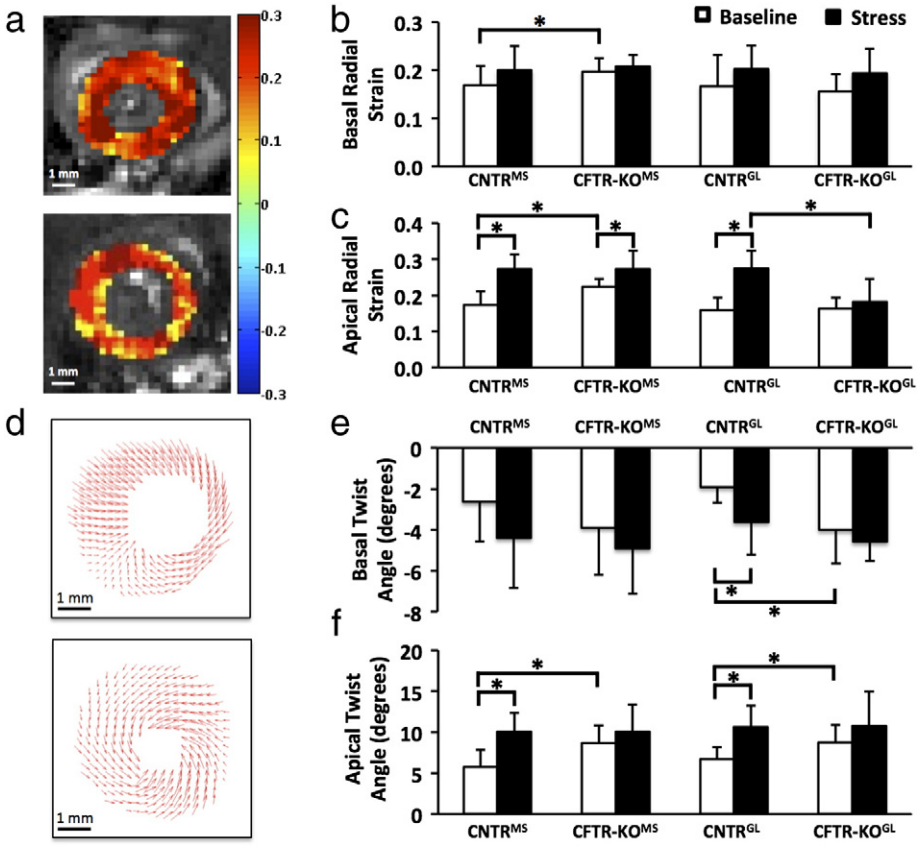

Fig. 2. **Radial strain and ventricular twist**. **a**. Representative radial strain maps in CFTR-KO^{MS} (**upper**) and CNTR^{MS} (**lower**) mice at peak systole. **b&c**. Average basal (**b**) and apical (**c**) radial strain at peak systole. **d**. Representative displacement maps in basal (**upper**) and apical (**lower**) slices at peak systole. **e&f**. Average basal (**b**) and apical (**c**) ventricular twist at peak systole. *P < 0.05.

ventricular torsion (Fig. 3). At baseline, peak twist at apex was significantly increased in the CFTR-KO^{MS} mice (Fig. 2f, $p < 0.05$). As a result, LV torsion and peak systolic torsion rate were significantly increased in the CFTR-KO^{MS} mice (Fig. 3, $p < 0.05$). Similarly, the CFTR-KO^{GL} mice also showed increased twist, torsion, and peak systolic torsion rate at baseline (Figs. 2e&f and 3, $p < 0.05$).

β-stimulation induced a significant increase in peak apical twist in CNTR^{MS} mice ($p < 0.05$). Peak torsion increased significantly in both CFTR-KO^{MS} mice and their control littermates, with the control mice showing a greater percentage increase as compared to the baseline. As a result, there was no difference in ventricular twist and torsion between CFTR-KO^{MS} mice and their controls under β-stimulation. The CFTR-KO^{GL} mice also showed similar response to β-stimulation as compared to their control littermates.

3.4. Cardiomyocyte Contractility and Ca^{2+} Transients

Measured cardiomyocyte contractility and Ca^{2+} transients are shown in Fig. 4. Fractional shortening and time to peak shortening were similar between the CFTR-KO mice and their respective controls, both at baseline and under cardiac stress. Ca^{2+} transients were also similar for all four groups both at baseline and under stress. Ca^{2+} decay constant was significantly decreased in the CFTR-KO^{MS} mice as compared to the controls at baseline, but was similar under cardiac stress. There was no difference in Ca^{2+} decay constant between the CFTR-KO^{GL} mice and the controls.

4. Discussion

In the current study, we investigated the impact of CFTR on cardiac function in two mouse models with CFTR disruption. The study on the CFTR-KO^{MS} mice evaluated the impact of CFTR disruption on cardiac function without the confounding factors from CF-induced systemic disorders. Our results show that CFTR disruption led to increased ejection fraction, radial strain, ventricular twist and torsion at baseline. The study on the CFTR-KO^{GL} mice investigated the impact of systemic CFTR disruption and the role of CF-related manifestations on cardiac function. The CFTR-KO^{GL} mice showed retarded growth and decreased LV size but normal ejection fraction. Similar to CFTR-KO^{MS} mice, CFTR-KO^{GL} mice also showed increased ventricular twist and torsion at baseline. Despite these observed changes *in vivo*, no differences were observed in myocyte contractility and Ca^{2+} transients.

Both the CFTR-KO^{MS} and CFTR-KO^{GL} mice showed an increase in regional baseline function such as twist and torsion. However, the CFTR-KO^{GL} mice showed a decrease in global functional parameters such as heart rate, stroke volume, and cardiac output, while these parameters were similar to the controls for CFTR-KO^{MS} mice. This difference can be attributed to the retarded growth of the CFTR-KO^{GL} mice. The body weight of the CFTR-KO^{GL} mice was 21% lower than the controls. As result, the demand for blood supply is significantly lower than the CFTR-KO^{MS} mice.

Comparing to the global functional parameters, the analysis of the regional myocardial wall motion by MRI has been recognized as a more sensitive measure of early-stage

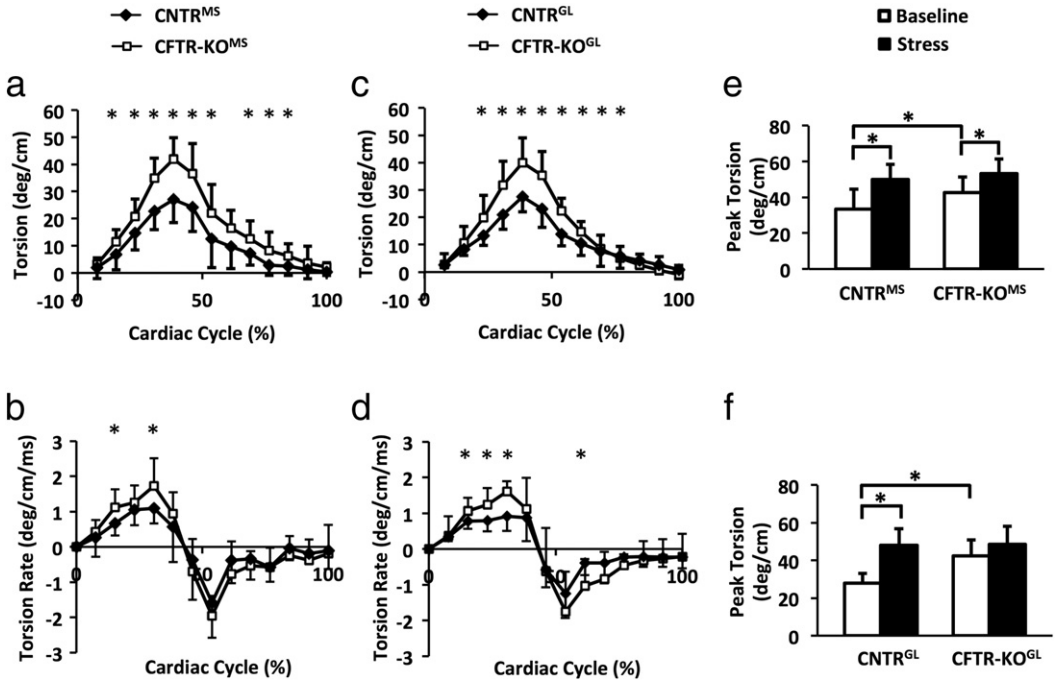

Fig. 3. **Ventricular torsion**. **a-d**. Time courses of ventricular torsion (**a&c**) and torsion rate (**b&d**) in one cardiac cycle in CFTR-KO^{MS} (**a&b**) and CFTR-KO^{GL} (**c&d**) mice and their respective controls at baseline. **e&f**. Average torsion at peak systole in CFTR-KO^{MS} (**e**) and CFTR-KO^{GL} (**f**) mice and their respective controls. *P < 0.05.

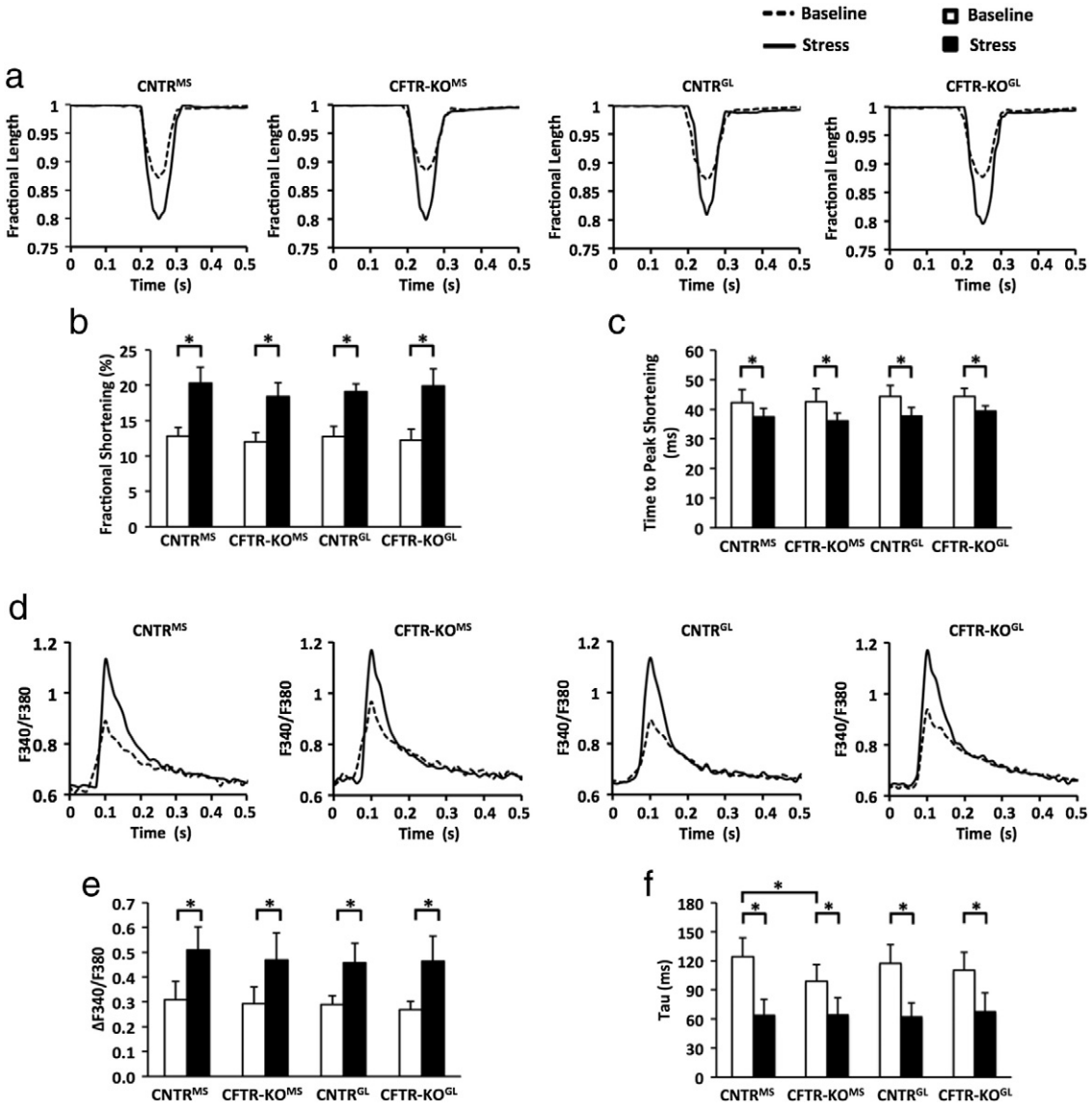

Fig. 4. **Cardiomyocyte contractility and Ca^{2+} transients**. **a**. Representative time courses of changes in cell length at baseline and under stress in all groups. **b**. Fractional shortening. **c**. Time to peak shortening. **d**. Representative time courses of Ca^{2+} transients at baseline and under stress in all groups. **e**. Peak Ca^{2+} transients. **f**. Ca^{2+} decay constant. *P < 0.05.

functional alterations, especially for changes in twist and torsion, which has been shown to be early signs of myocardial dysfunction [22]. The current MRI study suggests that CFTR disruption induced an increase in baseline myocardial contractility *in vivo*, in the absence of changes in myocyte contractility and the magnitude of Ca^{2+} transients. Previously, Sellers and colleagues reported increased peak LV pressure and pressure rate at both systole and diastole in CF mice, also suggesting increased myocardial contractility *in vivo* [17]. In addition, they also observed decreased aortic diameter and increased aortic stiffness by echocardiography. In the current study, we also observed a similar decrease in aortic diameter by MRI. This decrease in aortic diameter and increase in aortic stiffness suggest increased LV afterload in CFTR-KO mice. Hence, the observed increase in myocardial contractility *in vivo* can be an adaptation to the increased afterload in order to maintain normal cardiac output. However, the mechanisms leading to aortic constriction and stiffness need further investigation.

In addition to increased myocardial contractility, CFTR-KO^{MS} mice also showed an increase in the rate of ventricular filling at early diastole at baseline. Previously, Sellers and colleagues observed increased dP/dt at diastole in ΔF508 mice [15]. Consistent with these *in vivo* observations, isolated myocytes from the CFTR-KO^{MS} mice showed a significant decrease in Ca^{2+} decay constant at baseline, suggesting increased Ca^{2+} uptake by the sarcoplasmic reticulum. Previously, Sellers et al. reported that cardiac myocytes in neonatal CFTR-KO mice require the activation of Ca^{2+}/calmodulin-dependent kinase II (CaMKII) and calcium-activated chloride channels (CACC) to maintain contraction rate [16]. In the current study, the increased Ca^{2+} uptake by the sarcoplasmic

reticulum may be a downstream effect of the activation of CaMKII. However, it remains to be elucidated whether there is increased activity of CaMKII and CACC in the CFTR-KO^{MS} mice. In contrast to the CFTR-KO^{MS} mice, the CFTR-KO^{GL} mice showed no change in Ca^{2+} decay constant but a slight decrease in ventricular filling rate, possibly due to a smaller ventricular volume associated with the retarded growth of CFTR-KO^{GL} mice.

Contrary to the increased myocardial contractility at baseline, the *in vivo* response of CFTR-KO mice to β-adrenergic stimulation was either similar to their corresponding controls or slightly attenuated. As such, the percentage change relative to baseline appeared lower in CFTR-KO mice than in their control littermates, primarily due to an increase in baseline contractility. Previously, Sellers et al. also reported diminished changes from baseline in LV pressure, +dP/dt, and − dP/dt in responses to β-stimulation in ΔF508 mice [15]. In the current study, we evaluated the contractile reserve of CFTR-KO mice by measuring the fractional shortening and Ca^{2+} transients of the isolated myocytes under isoproterenol stimulation. The lack of difference between the CFTR-KO myocytes and the controls suggest that the sensitivity to β-stimulation and the Ca^{2+} reserve in sarcoplasmic reticulum were preserved in CFTR-KO myocytes. Further, the similar increases in fractional shortening indicate that the cross-bridge cycling and myofilament Ca^{2+} sensitivity were also unaltered in our CFTR-KO mice. Hence, the slightly attenuated response to β-adrenergic stimulation *in vivo* may have also been caused by the elevated afterload, which diminished the contractile capacity of the myocardium under stress. Previous clinical studies have reported attenuated response to exercise in CF patients. Specifically, CF patients with normal LV ejection fraction at rest showed compromised ejection fraction under stress [24,25]. Although the adverse effects from pulmonary diseases cannot be excluded, our current results indicate that changes in aortic structure and tissue properties may also play a role.

Previous studies have reported abnormal Ca^{2+} homeostasis and increased Ca^{2+} store in the endoplasmic reticulum (ER) of the F508del-CFTR epithelial cells [26,27]. Two possible mechanisms have been proposed: the inositol 1,4,5-trisphosphate receptors (IP3Rs)-dependent Ca^{2+} release [28] and the transient receptor potential canonical channel 6 (TRPC6)-dependent-Ca^{2+} influx [29]. The unaltered Ca^{2+} transients and reserve in both CFTR-KO models observed in our current study suggest that these mechanisms are unlikely involved in the regulation of Ca^{2+} homeostasis in cardiac myocytes.

Besides CFTR, recent studies have investigated the functional roles of several other Cl^- channels, such as the ClC voltage-gated Cl^- channels including ClC-2 and ClC-3, in murine hearts [30–32]. In ClC-2 knockout mice, Huang et al. observed that the targeted inactivation of ClC-2 prevented the positive chronotropic effect of acute exercise stress through a sympathetic regulation of ClC-2 channels [31]. In contrast, CFTR knockout did not blunt the stress-induced increase in heart rate in our current study. Recently, Xiong et al. investigated the physiological role of ClC-3 in cardiac function. They observed dramatically reduced ejection fraction and fractional shortening, as well as severe signs of myocardial hypertrophy and heart failure in the mice with cardiac-specific knockout of ClC-3 [32]. However, CFTR knockout did not give rise to such severe cardiac dysfunction. The mechanisms leading to the diverse phenotypes of these Cl^- channel knockout mice need to be further investigated.

We did not observe a difference in wall thickness between the CFTR-KO^{MS} mice and their control littermates. However, Sellers et al. reported a significant increase in the posterior and septal wall thickness in 4 ~ 5 month ΔF508 mice [17]. One possible reason for this difference could be that the mice characterized in our current study were at a younger age (~2 months). As the CFTR-KO^{MS} mice age, the elevated myocardial contractility can lead to mild LV hypertrophy. However, future studies are needed to investigate the chronic impact of CFTR disruption on cardiac function.

One limitation of the current study is that it is not possible to distinguish between cardiac and vascular effects since CFTR knockout affects both the cardiac and smooth muscle cells. Future studies on mice with cardiac-specific knockout of CFTR will allow us to gain insight into the roles of CFTR in myocytes only. The current study allowed us to assess the effects of systemic and tissue-specific CFTR knockout on cardiac function at both the organ and the cellular levels in the absence of lung diseases. These findings will enhance our understanding of the progression of cardiac dysfunction in CF patients.

In conclusion, CFTR disruption leads to increased LV regional function at baseline, as well as a slightly attenuated response to β-adrenergic stimulation in young CFTR-KO mice which are absent of pulmonary infection and exacerbation. These observations suggest that chronically elevated myocardial contractility at baseline may render the hearts of CF patients more susceptible to untoward remodeling processes that will eventually lead to abnormal LV function that is independent of lung disease.

Funding sources

This study was supported by NIH Grants HL73315 (Yu).

Disclosures

None.

Acknowledgements

We would like to thank the Case Western Reserve CF Mouse Models Core (P30 DK27651) for producing the mice used in this study.

Appendix A. Supplementary data

Supplementary data to this article can be found online at http://dx.doi.org/10.1016/j.jcf.2015.06.003.

References

[1] Lubamba B, Dhooghe B, Noel S, Leal T. Cystic fibrosis: insight into CFTR pathophysiology and pharmacotherapy. Clin Biochem 2012;45: 1132–44.

[2] Guggino WB, Stanton Ba. New insights into cystic fibrosis: molecular switches that regulate CFTR. Nat Rev Mol Cell Biol 2006;7:426–36.

[3] Cohen-Cymberknoh M, Shoseyov D, Kerem E. Managing cystic fibrosis: strategies that increase life expectancy and improve quality of life. Am J Respir Crit Care Med 2011;183:1463–71.

[4] Duan D, Ye L, Britton F, Miller LJ, Yamazaki J, Horowitz B, et al. Purinoceptor-coupled Cl- channels in mouse heart: a novel, alternative pathway for CFTR regulation. J Physiol 1999;521(Pt 1):43–56.

[5] Tilly BC, Bezstarosti K, Boomaars WE, Marino CR, Lamers JM, de Jonge HR. Expression and regulation of chloride channels in neonatal rat cardiomyocytes. Mol Cell Biochem 1996;157:129–35.

[6] Gao Z, Sun H-Y, Lau C-P, Chin-Wan Fung P, Li G-R. Evidence for cystic fibrosis transmembrane conductance regulator chloride current in swine ventricular myocytes. J Mol Cell Cardiol 2007;42:98–105.

[7] Warth JD, Collier ML, Hart P, Geary Y, Gelband CH, Chapman T, et al. CFTR chloride channels in human and simian heart. Cardiovasc Res 1996; 31:615–24.

[8] Duan DD. Phenomics of cardiac chloride channels. Comput Physiol 2013; 3:667–92.

[9] Chen H, Liu LL, Ye LL, McGuckin C, Tamowski S, Scowen P, et al. Targeted inactivation of cystic fibrosis transmembrane conductance regulator chloride channel gene prevents ischemic preconditioning in isolated mouse heart. Circulation 2004;110:700–4.

[10] Solbach TF, Paulus B, Weyand M, Eschenhagen T, Zolk O, Fromm MF. ATP-binding cassette transporters in human heart failure. Naunyn Schmiedebergs Arch Pharmacol 2008;377:231–43.

[11] Ozcelik N, Shell R, Holtzlander M, Cua C. Decreased right ventricular function in healthy pediatric cystic fibrosis patients versus non-cystic fibrosis patients. Pediatr Cardiol 2013;34:159–64.

[12] Ionescu AA, Payne N, Obieta-Fresnedo I, Fraser AG, Shale DJ. Subclinical right ventricular dysfunction in cystic fibrosis. A study using tissue Doppler echocardiography. Am J Respir Crit Care Med 2001;163: 1212–8.

[13] Eckles M, Anderson P. Cor pulmonale in cystic fibrosis. Semin Respir Crit Care Med 2003;24:323–30.

[14] Labombarda F, Pellissier A, Ellafi M, Creveuil C, Ribault V, Laurans M, et al. Myocardial strain assessment in cystic fibrosis. J Am Soc Echocardiogr 2011;24:1037–45.

[15] Hodges CA, Cotton CU, Palmert MR, Drumm ML. Generation of a conditional null allele for Cftr in mice. Genesis 2008;46:546–52.

[16] Sellers ZM, De Arcangelis V, Xiang Y, Best PM. Cardiomyocytes with disrupted CFTR function require CaMKII and Ca(2+)-activated Cl(-) channel activity to maintain contraction rate. J Physiol 2010;588: 2417–29.

[17] Sellers ZM, Kovacs A, Weinheimer CJ, Best PM. Left ventricular and aortic dysfunction in cystic fibrosis mice. J Cyst Fibros 2013;12:517–24.

[18] Zhong J, Yu X. Strain and torsion quantification in mouse hearts under dobutamine stimulation using 2D multiphase MR DENSE. Magn Reson Med 2010;64:1315–22.

[19] Snouwaert JN, Brigman KK, Latour AM, Malouf NN, Boucher C, Smithies O, et al. Animal Fibrosis Made for Model by Gene Cystic Targeting. 2014;257:1083–8.

[20] Holtwick R, Gotthardt M, Skryabin B, Steinmetz M, Potthast R, Zetsche B, et al. Smooth muscle-selective deletion of guanylyl cyclase-A prevents the acute but not chronic effects of ANP on blood pressure. Proc Natl Acad Sci U S A 2002;99:7142–7.

[21] Zhong J, Yu X. Strain and torsion quantification in mouse hearts under dobutamine stimulation using 2D multiphase MR DENSE. Magn Reson Med 2010;64:1315–22.

[22] Li W, Liu W, Zhong J, Yu X. Early manifestation of alteration in cardiac function in dystrophin deficient mdx mouse using 3D CMR tagging. J Cardiovasc Magn Reson 2009;11:40.

[23] Moaveni S. Finite element analysis—theory and application with ANSYS. 1999;12.

[24] Chipps BE, Alderson PO, Roland JM, Yang S, van Aswegen A, Martinez CR, et al. Noninvasive evaluation of ventricular function in cystic fibrosis. J Pediatr 1979;95:379–84.

[25] Benson LN, Newth CJ, DeSouza M, Lobraico R, Kartodihardjo W, Corkey C, et al. Radionuclide assessment of right and left ventricular function during bicycle exercise in young patients with cystic fibrosis. Am Rev Respir Dis 1984;130:987–92.

[26] Antigny F, Norez C, Becq F, Vandebrouck C. Calcium homeostasis is abnormal in cystic fibrosis airway epithelial cells but is normalized after rescue of F508del-CFTR. Cell Calcium 2008;43:175–83.

[27] Martins JR, Kongsuphol P, Sammels E, Dahimène S, Aldehni F, Clarke LA, et al. F508del-CFTR increases intracellular Ca(2+) signaling that causes enhanced calcium-dependent Cl(-) conductance in cystic fibrosis. Biochim Biophys Acta 1812;2011:1385–92.

[28] Antigny F, Norez C, Cantereau A, Becq F, Vandebrouck C. Abnormal spatial diffusion of Ca2+ in F508del-CFTR airway epithelial cells. Respir Res 2008;9:70.

[29] Antigny F, Norez C, Dannhoffer L, Bertrand J, Raveau D, Corbi P, et al. Transient receptor potential canonical channel 6 links Ca2+ mishandling to cystic fibrosis transmembrane conductance regulator channel dysfunction in cystic fibrosis. Am J Respir Cell Mol Biol 2011;44:83–90.

[30] Duan D. Phenomics of cardiac chloride channels: the systematic study of chloride channel function in the heart. J Physiol 2009;587:2163–77.

[31] Huang ZM, Prasad C, Britton FC, Ye LL, Hatton WJ, Duan D. Functional role of CLC-2 chloride inward rectifier channels in cardiac sinoatrial nodal pacemaker cells. J Mol Cell Cardiol 2009;47:121–32.

[32] Xiong D, Heyman NS, Airey J, Zhang M, Singer CA, Rawat S, et al. Cardiac-specific, inducible ClC-3 gene deletion eliminates native volume-sensitive chloride channels and produces myocardial hypertrophy in adult mice. J Mol Cell Cardiol 2010;48:211–9.